INTERNATIONAL JOURNAL FOR NUMERICAL METHODS IN FLUIDS
Int. J. Numer. Meth. Fluids 2011; **67**:1283–1290
Published online 7 October 2010 in Wiley Online Library (wileyonlinelibrary.com). DOI: 10.1002/fld.2418

Radial basis function neural network model for mean velocity and vorticity of capillary flow

Mostafa Y. El-Bakry*, †

Physics Department, Faculty of Science, Benha University, Egypt

SUMMARY

The radial basis function neural network (RBFNN) simulation has been designed to simulate and predict the mean velocity of capillary flow in transition from laminar to turbulent flow and the root-mean-square vorticity as a function of wall-normal position at different values of Reynolds number. The system was trained on the available data of the two cases. Therefore, we designed the system to work in automatic way for finding the best network that has the ability to have the best test and prediction. The proposed system shows an excellent agreement with that of an experimental data in these cases. The technique has been also designed to simulate the other distributions not presented in the training set and predicted them with effective matching. Copyright © 2010 John Wiley & Sons, Ltd.

Received 31 May 2010; Revised 2 August 2010; Accepted 8 August 2010

KEY WORDS: neural networks; radial basis function neural network; mean velocity; vorticity; laminar flow; capillary flow

1. INTRODUCTION

There are a variety of practical applications, ranging from drug-delivery and bioanalyses systems to the implementation of efficient thermal management strategies for microelectronics cooling, that require an understanding of fluid flow at the microscale [1]. In particular, a subset of these applications, like enhanced heat transfer for microelectronic cooling applications [2] and passive mixing in chemical microreactors [3], relies heavily on the characteristics of flow in the transitional and turbulent regimes.

There is an existence of the similarity and the difference between transitional flows at the micro- and macro-scales.With regard to transition to turbulence at the microscale, the results of many groups have indicated that this transition occurs at anomalously low Reynolds number (Re) in comparison to macroscale transition. Observations were made for flow in rectangular microchannels of varying aspect ratios where single-point statistics, calculated from velocity fields acquired by micro-PIV, revealed the onset of transition at $Re \sim 1800$–2300 [4].

In general, experimental studies of transitional flows at the microscale are often limited to the measurement of bulk flow parameters [3, 4], such as flow rate and frictional pressure-drop along the length of the channel. With the development of microscopic PIV as a tool for obtaining spatially resolved velocity fields at the microscale [5, 6], there is growing interest in studying the underlying characteristics of complex flow features at the microscale. In a typical micro-PIV experiment, the flow is volume illuminated and the spatial resolution in the depth direction is defined by the imaging optics. Consequently, particles that are just beyond the depth of focus

*Correspondence to: Mostafa Y. El-Bakry, Physics Department, Faculty of Science, Benha University, Egypt.
†E-mail: oelbakre@yahoo.com

appear as noise in the acquired images [7]. Therefore, it has become customary to drastically reduce the particle seeding density in micro-PIV experiments and instead utilize ensemble-averaging of correlation functions to obtain accurate and well-resolved velocity vector fields [6]. In this form, however, micro-PIV is inherently limited to the measurement and visualization of steady flows or the mean characteristics of unsteady flows (including periodic flows wherein the measurements can be accurately phase-locked to the periodic flow physics). In contrast, the accurate measurement of instantaneous unsteady and/or turbulent flow physics requires the acquisition of highly resolved, instantaneous velocity fields which demands the use of a relatively high seeding density.

The first measurements of transition and turbulence via micro-PIV were reported by Li *et al.* [4, 8] for flow through rectangular PDMS microchannels. They concluded that fully developed turbulent flow was achieved at Reynolds numbers between 2600 and 2900 based on analysis of the streamwise and wall-normal root-mean-square (RMS) velocities and the Reynolds shear stresses. The examination of large-scale turbulent structures in rectangular PDMS microchannels with varying aspect ratios using spatial correlations of the velocity fluctuations are reported in [9]. Most recently, micro-PIV measurements in the streamwise-wall-normal plane of a 536 lm capillary at $Re = 4500$ by Natrajan *et al.* [10] showed the singlepoint statistics, including profiles of the mean velocity, the RMS streamwise and wall-normal velocities and the Reynolds shear stress, to be in good agreement with that observed in a direct numerical simulation (DNS) of turbulent pipe flow at a comparable Re. Validation of the efficacy of micro-PIV as an experimental tool for resolving the instantaneous velocity fluctuations that occur in wall-bounded turbulent flows are established [10].

Given the conflicting evidence that exists regarding pathways of transition to turbulence at the microscale, the underlying physics of these flows must be understood before microfluidic devices that operate in this regime can be optimized for increased performance and efficiency, particularly from a heat-transfer standpoint.

The characteristics of transitional wall-bounded flows at the microscale via pressure-drop and micro-PIV measurements of flow through a 536 lm diameter capillary over a broad range of Re are documented in [11]. Measurements are conducted from $Re = 1800$ to 3400 to study the bulk and spatial characteristics of the flow as it undergoes transition from a laminar to a turbulent state in microscale capillaries.

The present effort introduces the artificial neural network (ANN) for modeling the mean velocity and the vorticity of transitional flow in microscale capillaries using the data obtained from Natrajan and Christensen [11].

Neural networks are widely used for solving many problems in most science problems of linear and nonlinear cases [12–20]. Neural network algorithms are always iterative, designed to step by step minimize (targeted minimal error) the difference between the actual output vector of the network and the desired output vector [21–23].

Radial basis function neural network (RBFNN) is a feed-forward neural network with good performance, and the speed of training methods is high. The model is not only simple but also with higher precision and purpose capabilities, and it has a strong biological background and close arbitrary nonlinear function of capacity. Therefore, it has been paid more attention to in recent years. Radial basis function (RBF) neural network is based on supervised learning. RBF networks were independently proposed by many researchers [24–26] and are a popular alternative to the multilayer perceptron (MLP). RBF networks are also good at modeling nonlinear data and can be trained in one stage rather than using an iterative process as in MLP and also learn the given application quickly. They are useful in solving problems.

The data obtained by Natrajan and Christensen [11] are chosen to be carried out using the RBF neural networks.

The present work offers an efficient RBF neural network that is used to simulate and predict the unknown data of the RMS vorticity σ_{λ} and the mean velocity $U(r)$ as a function of wall-normal position r/R at different values of Reynolds number ranging in transition from laminar to turbulent flow in capillary flow.

DOI: 10.1002/fld

The rest of the paper is organized as follows: Section 2 describes the trained NN. Section 3 presents the proposed system. Section 4 shows the obtained results. Finally, Section 5 concludes the work.

2. RBFNN OVERVIEW

In this paper, we will use another type of neural networks: the radial basis function networks (or RBFN) [24–26]. These networks have the advantage of being much simpler than the perceptrons while keeping the major property of universal approximation of functions [26]. RBFNNs rank among the most popular tools for function approximation and have currently been widely applied in many areas, such as nonlinear control, speech processing and pattern recognition [25]. An RBFN is an artificial neural network that uses RBFs as activation functions. Although several forms of radial basis may be used, Gaussian kernels are most commonly used.

The basic architecture of an RBF network with inputs and a single output is shown in Figure 1. The RBFN model consists of three layers: an input layer, a hidden (kernel) layer and an output layer, as shown in Figure 1. The nodes within each layer are fully connected to the previous layer. The input variables are each assigned to a node in an input layer and pass directly to the hidden layer without weights. The hidden nodes or units contain the RBF, also called transfer functions.

Given a set of data points, $\{X_i, Y_i\}_{i=1}^{i=N}$, where the vector X is an input, vector Y is the desired output and N is the number of training pairs. Based on the RBFNN, it is desired to construct an approximation function $\hat{Y} = f(X) \cong Y$ that minimizes an error function E over the given training set. This approximation function $f(X)$ is assumed to be a linear weighted sum of radially symmetric function of X. Such RBFNN network can be represented by the following model:

$$f(X) = \sum_{j=1}^{m} w_{kj} \phi_j(\|x - c_j\|) \tag{1}$$

where w_{kj} is the synaptic weight connecting hidden neuron j to output neuron k, $\phi_j(.)$ is a Gaussian kernel of the hidden neuron j, $\|\cdot\|$ denotes the Euclidean norm, c_j is the center of the jth kernel and m is the total number of kernels. The Gaussian kernel $\phi_j(.)$ is defined as

$$\phi_j(\|X - c_j\|) = \mathrm{e}^{-\|X - c_j\|^2/\sigma_j} \tag{2}$$

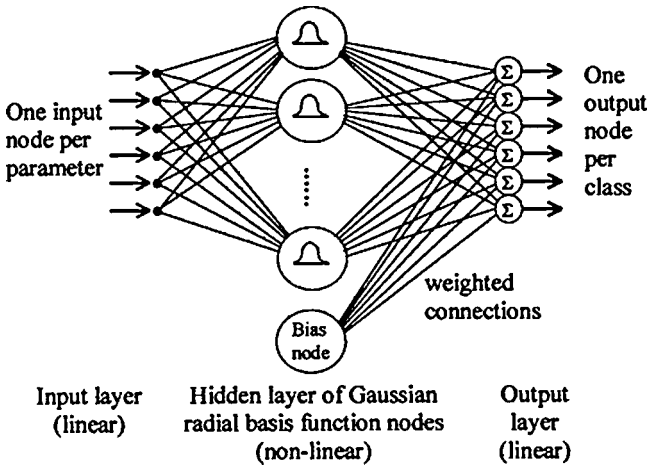

Figure 1. The radial basis function neural network.

DOI: 10.1002/fld

where σ_j is the width of the jth kernel. The problem of RBF approximation is to find appropriate centers c_j's and widths σ_j's of the hidden nodes and weights w_{kj}'s of the linear layer. The degree of accuracy of the RBF networks can be controlled by these three parameters.

The sum of squared error criterion function can be considered as an error function E to be minimized over the given training set. That is, to develop a training method that minimizes E by adaptively updating the three parameters of the RBF network.

Training RBF ANN occurs in two separate stages (unsupervised stage and supervised stage). The first stage is subdivided into two steps: selection of the basis function centers (this is determined by some sort of clustering), followed by selection of the width of each basis function (this is determined by a k-nearest neighbor method). In the second stage, the weights between the hidden and the output layers are computed using the pseudo-inverse method for a constant value of σ as given as follows:

$$\phi W = Y \tag{3}$$

$$W = \phi^{-1} Y \tag{4}$$

$$W = [(\varphi^{\mathrm{T}}\phi)^{-1}\phi^{\mathrm{T}}]Y \tag{5}$$

where ϕ, W and Y denote ϕ_j, w_{kj} and the output in matrix form, respectively.

The approximated output $\hat{Y}$ is shown in the following equation:

$$\hat{Y} = f(X, c, \sigma, W) = \sum_{j}^{m} w_{kj}\phi_j(X, c_j, \sigma_j) \tag{6}$$

3. THE PROPOSED RBF NEURAL NETWORK SYSTEM

The studied problem consists of two parts: the first part (RBFNN1) simulates the root mean vorticity σ_λ and the second one (RBFNN2) models the mean velocity $U(r)$, which depends on the function of the wall-normal position r/R. Each part contains four groups of data corresponding to four different Reynolds numbers that are in the range of transition from laminar to turbulent flow. These numbers are $Re = 2000$, 2300, 2600 and 2900.

Three groups are chosen as patterns for training ($Re = 2000$, 2300 and 2600) and one group for prediction ($Re = 2900$). Our problem has two inputs (wall-normal position and Reynolds number) and single output (for RBFNN1 model and $U(r)$ for RBFNN2 model) in each part.

We have preferred to use the same neural network architecture in the two cases. It was found that one hidden layer and 10 neurons are enough for reaching the optimal solution. Figure 2 shows a block diagram of this model in two cases. We first set up the network with random weights and biases values.

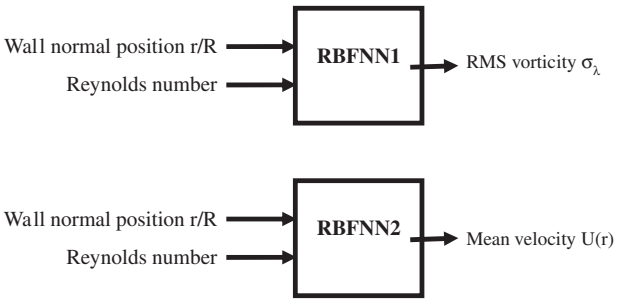

Figure 2. A block diagram modeling.

DOI: 10.1002/fld

The performance of the previous two models is examined by using the mean square error (MSE) and the mean absolute error (MAE), which are defined as follows:

$$\mathrm{MSE} = \frac{1}{N}\sum_{i=1}^{N}\left(E_{i_{\mathrm{measured}}} - E_{i_{\mathrm{predicted}}}\right)^2 \tag{7}$$

$$\mathrm{MAE} = \frac{1}{N}\sum_{i=1}^{N}\left|\left(E_{i_{\mathrm{measured}}} - E_{i_{\mathrm{predicted}}}\right)\right| \tag{8}$$

In Equations (7) and (8), E denotes the RMS vorticity σ_λ and λ is swirling strength of the velocity gradient tensor in first case and mean velocity $U(r)$ in second case and N is the total number of data.

The optimal RBFNN parameters (the number of RBF and center c_j's and width σ_j's of each RBF) were determined by experiments with a number of trials by taking into account the error measurements. In general, a good model will produce less error measurements (in our case MSE and MAE). The MSE and MAE were calculated for both the training and testing (prediction) data sets for different number of hidden nodes to avoid the over-fitting problem. The error calculated using the testing data set often provides a better measurement of the predictive capability of a fitted model. Thus, computing the error over the testing data set becomes more helpful to validate the model and avoid over-fitting.

4. RESULTS

The proposed RBFNN models were applied to simulate the experimental data [11] of the vorticity (referred to as model 1) and mean velocity (model 2). By employing the above-mentioned proposed models with different values of the RBF parameters (c and w), we have obtained different numbers of hidden neurons for the RBFNN models. The results obtained by the two models are discussed in the following subsections.

4.1. RMS vorticity (model 1)

The RBFNN is used in this research with two input nodes (r/R and Re), one hidden layer with 32 nodes and a single output node (σ_λ) designed as a '2-32-1' net. The selection of the optimal width value for RBFNN was performed by systemically changing its value in the training step. The value that gives a minimum error was chosen as the optimal value and was used in the model. The adjustment of the connection weight between the hidden and the output layers was performed using a least-squares solution after the selection of centers and width of RBFNN1. The overall performance of RBFNN1 is evaluated in terms of a MSE and MAE. For this model, the optimal width value was ranged between 0.00323 and 0.3465. The corresponding number of centers (hidden layer nodes) of RBFNN1 is 32. Therefore, an RBFNN1 with '2-32-1' structure was developed.

In the prediction model, we find that a value of 32 centers and a radius range (0.00323–0.34650) lambda range (0.00585–0.09762) will give the optimal error results for the model. The optimum number of functional centers was determined by assessing the relative performance of the one-step ahead prediction model using a range of values for the number of centers.

Figure 3 shows the simulated results ($Re = 2000$, 2300 and 2600) and the predicted ones ($Re = 2900$). This figure also shows an exact matching between the calculated and predicted data with the experimental ones. According to model 1, we have obtained MSE = 0.0000758 and MAE = 0.00637207 for the predicted data.

4.2. Mean velocity (model 2)

The RBFNN2 has two inputs (r/R and Re) and one output layer unit ($u(r)$) and one hidden layer of 18 units. RBFNN2 can be designed as 2-18-1 net to indicate the number of units in input (2), hidden layer (18) and output layer (1), respectively. RBFNN2 is completely specified by choosing its parameters (the number of 18 of RBF and center c_j's ranged from 0.00147 to 1,424,405) and

DOI: 10.1002/fld

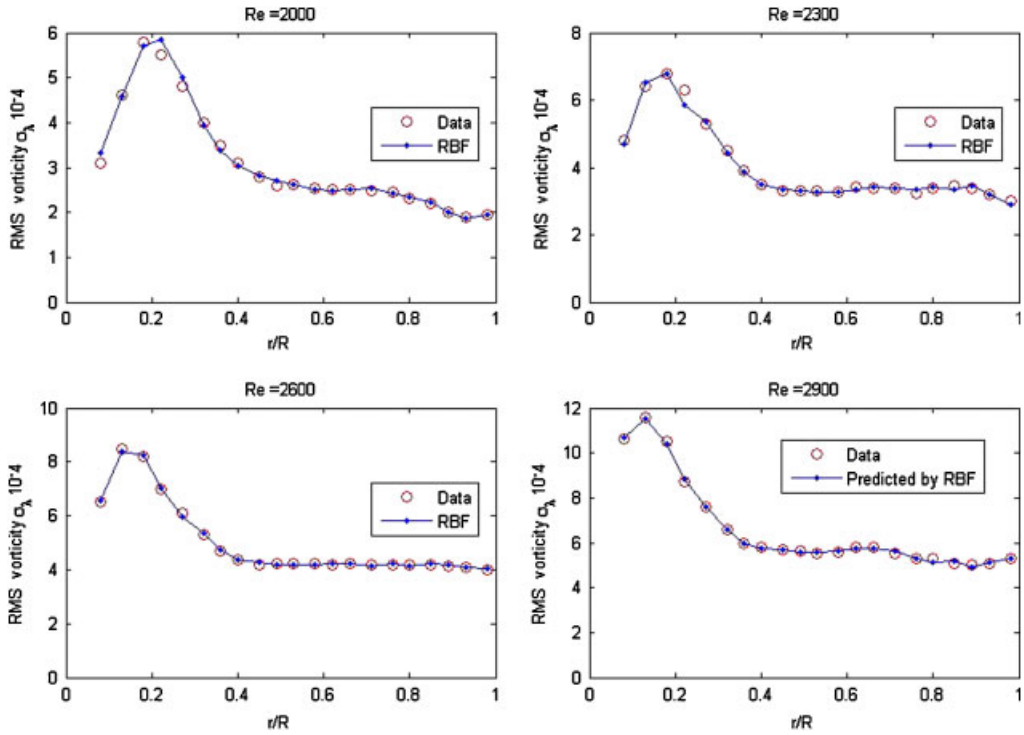

Figure 3. The RBFNN1 results of the root-mean-square vorticity.

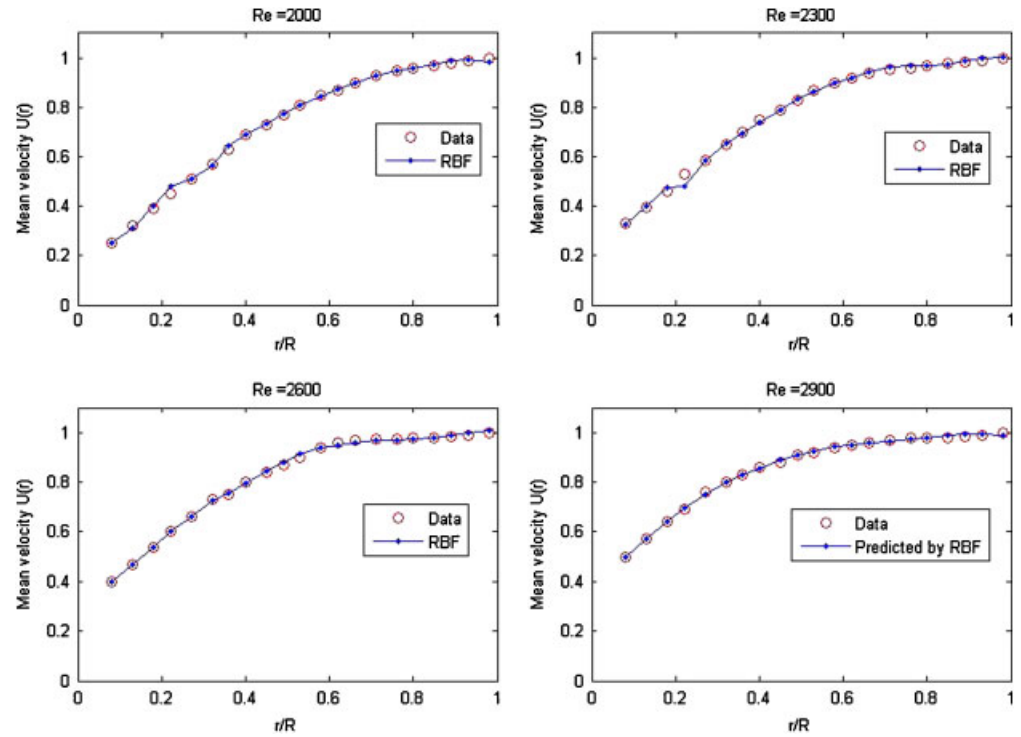

Figure 4. The RBFNN2 results of the mean velocity $U(r)$.

DOI: 10.1002/fld

width σ_j's of each RBF and the connection weights w_{kj}'s between jth hidden layer unit and kth output unit.

Figure 4(a)–(c) represents the simulation results ($Re = 2000$, 2300 and 2600) and the predicted model ($Re = 2900$) of mean velocity $u(r)$, which shows almost exact fitting to the given experimental data. The obtained model had an MSE = 0.0000745 and MAE = 0.005553 for the predicted data.

5. CONCLUSION

In this paper, a method was proposed to model the RMS vorticity σ_λ and the mean velocity $U(r)$ of capillary flow in transition from laminar to turbulent flow as a function of wall-normal position at different values of Reynolds number using RBFNNs. The trained RBFN shows excellent results matched with the experimental data in the two cases of the RMS vorticity σ_λ and the mean velocity $U(r)$. The RBFNN technique has been also designed to simulate the other distributions not presented in the training set and matched them effectively. Then, the capability of the RBFNN techniques to simulate and predict the experimental data with almost exact accuracy recommends the RBFFN to dominate the modeling techniques in physics of fluid.

REFERENCES

1. Gravesen P, Branebjerg J, Jensen OS. Microfluidics—a review. *Journal of Micromechanics and Microengineering* 1993; **3**:168–182.
2. Tuckerman DB, Pease RF. High-performance heat sinking for VLSI. *IEEE Electron Device Letters* 1981; **2**: 126–129.
3. Haswell SJ, Skelton V. Chemical and biochemical microreactors. *TrAC Trends in Analytical Chemistry* 2000; **7**:389–395.
4. Li H, Olsen MG. Aspect ratio effects in turbulent and transitional flow in rectangular microchannels as measured with micropiv. *Journal of Fluids Engineering* 2006; **128**:305–315.
5. Santiago JG, Wereley ST, Meinhart CD, Beebe DJ, Adrian RJ. A particle image velocimetry system for microfluidics. *Experiments in Fluids* 1998; **25**:316–319.
6. Meinhart CD, Wereley ST, Santiago JG. PIV measurements of a microchannel flow. *Experiments in Fluids* 2000; **27**:414–419.
7. Olsen MG, Adrian RJ. Out-of-focus effects on particle image visibility and correlation in microscopic particle image velocimetry. *Experiments in Fluids* 2000; **29**:S166–S174.
8. Li H, Ewoldt R, Olsen MG. Turbulent and transitional velocity measurements in a rectangular microchannel using microscopic particle image velocimetry. *Experimental Thermal and Fluid Science* 2005; **29**:435–446.
9. Li H, Olsen MG. Examination of large-scale structures in turbulent microchannel flow. *Experiments in Fluids* 2006; **40**(5):733–743.
10. Natrajan VK, Yamaguchi E, Christensen KT. Statistical and structural similarities between micro- and macro-scale wall turbulence. *Microfluidics and Nanofluidics* 2007; **3**:89–100.
11. Natrajan VK, Christensen KT. Microscopic particle image velocimetry measurements of transition to turbulence in microscale capillaries. *Experiments in Fluids* 2007; **43**:1–16.
12. El-Bakry MY, El-Bakry MY, Elhelly M. Neural network represntation for the forces and torque of the eccentric sphere model. *Transactions on Compututational Science III*. Lecture Notes in Computer Science, vol. 5300. Springer: Berlin, 2009; 171–183.
13. El-Bakry MY, El-Harby AA, Behery GM. Automatic neural network system for vorticity of square cylinders with different corner radii. *Journal of Applied Mathematics and Informative* (*JAMI*) 2008; **26**(5–6):911–923.
14. Elbakry MY, Radi A. Genetic programming approach for flow of steady state fluid between two eccentric spheres. *Applied Rheology* 2007; **17**(6):68210.
15. El Bakry MY, El-Metwally KA. Neural network for proton–proton collision at high energy. *Chaos*, *Solitons and Fractals* 2003; **16**(2):279–285.
16. El Bakry MY. Feed forward neural networks modeling for K–P interactions. *Chaos*, *Solitons and Fractals* 2003; **16**(2):279–285.
17. Hamid AK. Scattering from spherical shell with a circular aperture using neural networks approach. *Canadian Journal of Physics* 1998; **76**:63–67.
18. Scalabrin G, Corbetti C, Cristofoli G. A viscosity equation of state for R123 in the form of a multilayer feed forward neural network. *International Journal of Thermophysics* 2001; **22**(5):1383–1395.
19. El-dahshan E, Radi A, El-Bakry MY. Artificial neural network and genetic algorithm haybrid technique for nucleus–nucleus collisions. *International Journal of Modern Physics C* 2008; **19**:1787.
20. El-dahshan E, Radi A, El-Bakry MY. Genetic programming modeling for nucleus–nucleus collisions. *International Journal of Modern Physics C* 2009; **20**:1817.

DOI: 10.1002/fld

21. Hu Y-C, Tsai J-F. Backpropagation multi-layer perceptron for incomplete pairwise comparison matrices in analytic hierarchy process. *Applied Mathematics and Computation* 2006; **180**(1):53–62.
22. Curry B, Morgan PH. Model selection in neural networks: some difficulties. *European Journal of Operational Research* 2006; **170**(2):567–577.
23. Steil JJ. Online stability of backpropagation–decorrelation recurrent learning. *Neurocomputing* 2006; **69**(7–9): 642–650.
24. Karami A, Mohammadi MS. Radial basis function neural network for power system load-flow. *Electrical Power and Energy Systems* 2008; **30**:60–66.
25. Haykin S. *Neural Networks*: *A Comprehensive Foundation* (2nd edn). Prentice-Hall: Englewood Cliffs, NJ, 1999.
26. Refaee JA, Mohandes M, Maghrabi H. Radial basis function networks for contingency analysis of bulk power systems. *IEEE Transactions on Power Systems* 1999; **14**(2):772–778.

DOI: 10.1002/fld